6824 *Biochemistry* **2009,** *48,* 6824–6834
DOI: 10.1021/bi900488n

BIOCHEMISTRY
including biophysical chemistry & molecular biology
Article

Solution Structure of *S. cerevisiae* PDCD5-Like Protein and Its Promoting Role in H_2O_2-Induced Apoptosis in Yeast[†,‡]

Jingjun Hong, Jiahai Zhang, Zhijun Liu, Su Qin, Jihui Wu,* and Yunyu Shi*

Hefei National Laboratory for Physical Sciences at Microscale and School of Life Sciences, University of Science and Technology of China, Hefei 230027, P. R. China

Received March 24, 2009; Revised Manuscript Received May 25, 2009

ABSTRACT: Human PDCD5 protein is a novel programmed cell death-promoting molecule. However, the function of Ymr074cP, a *S. cerevisiae* homologue of hPDCD5, is still unknown. Heteronuclear NMR methods were used to determine the solution structure of the N-terminal 116-residue fragment (N116) of Ymr074cP protein. N116 is shown to be a heterogeneous ensemble of flexibly folded conformations, adopting an extended triple-helix bundle fold that is connected to a mobile but structured α-helix in the N-terminus by means of a lengthy highly flexible linker. By the nitroxide spin label, attached to the mutant cysteine residue at position 7 or 11, significant transient interactions were probed between the N-terminal helical portion and the core moiety plus several residues in the C-terminal tail. The topology of the triple-helix bundle is encoded mainly by hydrophobic interactions, and the N-terminal helical structure has a unique electrostatic potential character. A comparison of the solution structures of PDCD5-related proteins indicates that the structure of the triple-helix bundle is significantly conserved during evolution. We are the first to demonstrate that *YMR074c* overexpression promotes H_2O_2-induced apoptosis in yeast, not only in a metacaspase Yca1-dependent manner but also in a Yca1-independent manner and that deletion of the N-terminal helical portion greatly attenuates the apoptosis-promoting activity of this protein.

Programmed cell death 5 (PDCD5[1]) was originally identified from apoptotic TF-1 cells by the cDNA-representative differences analysis approach and is also known as TFAR19. It exhibits a ubiquitous expression pattern and its expression is upregulated in the apoptotic TF-1 cells (*1*). The 5′-upstream region of human *PDCD5* gene contains a highly active TATA-less promoter that is upregulated by etoposide (*2*). Human PDCD5 plays an important apoptosis-promoting role in some apoptotic tumor cells such as TF-1 (*1*), MGC-803 (*1*), Hela (*1*, *3*), and PC-3M-1E8 (*4*) cells. In addition, overexpression of h*PDCD5* also enhances caspase-independent paraptosis triggered by TAJ/TROY (*5*).

Ymr074cP is a single PDCD5 homologue in budding yeast. Up to now, in the *Saccharomyces* genome database, this protein has been described as an uncharacterized protein of unknown function. Here, we determined the solution structure of the N-terminal 116-residue fragment (N116) of Ymr074cP, Ymr074cP N116, by NMR spectroscopy. It was shown that the overall structure of N116 comprises two distinct structural regions: a structured N-terminal helix and a helical core connected by a highly disordered and flexible linker (constituted by 27 amino acid residues). We failed to characterize any long-range ($|i - j| \geq 5$) NOE connecting the N-terminal helix and the helical core. However, by introducing a paramagnetic probe, significant long-range interactions were probed between the N-terminal helical portion and the core moiety. A semiquantitative way, as used in ref *6*, was used to interpret the paramagnetic relaxation enhancement data, and the distance restraints were interpreted as average distances weighted for different conformations. It is clear that the object of this study should not be a single three-dimensional conformation but rather an ensemble of many conformations rapidly interconverting. In addition, we demonstrated

[†]This work was supported by the Chinese National Fundamental Research Project (Grants 2006CB806507 and 2006CB910200), the Chinese National Natural Science Foundation (Grants 30121001 and 30670426), and the Chinese National High-tech R&D Program (Grant 2006AA02A315).

[‡]The atomic coordinates of the final ensemble, together with the experimental distance and angle constraints, were deposited in the RCSB Protein Data Bank (accession codes 2FH0 (Δ81Δ) and 2JXN (N116)). The NMR assignments were deposited at the Biological Magnetic Resonance Data Bank (accession number 15562 (N116)).

*To whom correspondence should be addressed. (J.W.) Tel: 86-551-3603745. Fax: 86-551-3601443. E-mail: wujihui@ustc.edu.cn. (Y.S.) Tel: 86-551-3607464. Fax: 86-551-3601443. E-mail: yyshi@ustc.edu.cn.

[1]Abbreviations: CD, circular dichroism; CSP, chemical shift perturbation; EMSA, electrophoretic mobility shift assays; FITC, fluorescein isothiocynate; HSQC, heteronuclear single quantum coherence; IPTG, isopropyl-1-β-D-thiogalactoside; MES, 2-(*N*-morpholino)ethanesulfonic acid; MTSL, 1-oxyl-2,2,5,5-tetramethyl-3-pyrroline-3-methyl-methanethiosulfonate; NMR, nuclear magnetic resonance; NOEs, nuclear Overhauser effects; NOESY, NOE spectroscopy; PBEs, paramagnetic broadening effects; PDCD5, programmed cell death 5; PMSF, phenylmethanesulfonyl fluoride; rmsd, root-mean-square deviation; SDSL, site-directed spin labeling; TFAR19, TF-1 cell apoptosis-related gene 19; TOCSY, total correlation spectroscopy; TUNEL, TdT-mediated dUTP nick end labeling; Yca1, yeast caspase 1.

 Published on Web 05/26/2009

that overexpression of *YMR074*c promotes H_2O_2-induced apoptosis in yeast not only in a Yca1-dependent manner but also in a Yca1-independent manner and that the structural integrity of this protein is very important for playing its apoptosis-promoting role.

MATERIALS AND METHODS

Plasmid Construction, Protein Expression, and Purification. The DNA fragment encoding residues 1−116 of *S. cerevisiae* Ymr074cP (GenBank NP_013790), predicted as a double-stranded DNA-binding domain (PF01984) and designated hereafter as N116, was amplified by PCR and cloned into the expression vector pET-22b (Novagen) using the Nde I and Not I cloning sites. For purification purposes, a 6×His tag was added at the C-terminus of the construct. The construct was verified by DNA sequencing.

E. coli BL21 (DE3) cells (Novagen) were transformed with the recombinant plasmid for expression of the required protein product. For the production of uniformly ^{15}N or ^{13}C, ^{15}N-labeled samples, cells were grown in minimal medium containing 100 μg mL^{-1} of ampicillin and either $^{15}NH_4Cl$ (0.5 g L^{-1}) and glucose (2.5 g L^{-1}) or $^{15}NH_4Cl$ (0.5 g L^{-1}) and $^{13}C_6$-glucose (2.5 g L^{-1}), respectively. Recombinant protein expression was induced by the addition of IPTG to a final concentration of 0.3 mM, and the cells were grown for four hours at 37 °C.

The cells were harvested by centrifugation at 6000*g* for 10 min, resuspended in a lysis buffer (50 mM Tris-HCl, pH 7.8, 500 mM NaCl, and 1 mM PMSF), and lysed by sonication. The cell debris was removed by centrifugation at 14000*g* for 30 min. Protein was purified from the soluble protein fraction using Ni^{2+}-NTA resin (Pharmacia) and Superdex 75 size exclusion chromatography (Pharmacia), and then concentrated to 1 mM. Purity of the recombinant protein was confirmed by SDS−PAGE and mass spectrometry, and the concentration was estimated using BCA Protein Assay Kit (Pierce).

Also, the protein construct corresponding to residues 36−116 of Ymr074cP (designated hereafter as Δ81Δ) was cloned, expressed, and purified as described above.

Site-Directed Spin Labeling of Proteins. There is no cysteine residue in the amino acid sequence of N116. In order to introduce a nitroxide spin label, two single-cysteine mutants of N116, A7C, and A11C were constructed using site-directed mutagenesis. Subsequently, the spin label derived from MTSL (1-oxyl-2,2,5,5-tetramethyl-3-pyrroline-3-methylmethanethiosulfonate) was attached to the single cysteine residue in each cysteine variant via a thiol-specific reaction (*7*), and the spin-label mutants were designated hereafter as N116 A7C* and N116 A11C*. Uniform spin labeling was confirmed using mass spectrometry.

Far-UV CD Measurements. The far-UV CD spectrum for N116, N116 A7C*, or N116 A11C* (each sample with a final protein concentration of 10 μM; pH 6.0) was recorded on a Jasco J-810 spectropolarimeter at room temperature over the wavelength range from 190 to 250 nm in a 1 mm path-length cuvette using a scan speed of 100 nm/min. Three scans were averaged.

NMR Spectroscopy and Assignment. NMR samples of N116 (1 mM) or Δ81Δ (1 mM) were prepared in 20 mM sodium phosphate, pH 6.0, 50 mM NaCl, 1 mM EDTA, 0.05% (w/v) sodium azide, and 10% (v/v) D_2O. Spectra for sequential assignment and structure determination were recorded at 298 K at a ^1H frequency of 600.13 MHz on a Bruker Avance spectrometer using standard procedures (*8*). The data were collected with 200 × 1024 complex points in the ^{15}N and $^1H^N$ dimensions, respectively (^1H,^{15}N-HSQC); 50 × 120 × 1024 complex points in the ^{15}N, ^{13}C, and $^1H^N$ dimensions (CBCANH, CBCA(CO)NH, HNCO, and HN(CA)CO); 50 × 160 × 1024 complex points in the ^{15}N, ^1H, and $^1H^N$ dimensions (HBHA(CBCACO)NH); 50 × 256 × 1024 complex points in the ^{15}N, ^1H, and $^1H^N$ dimensions (^{15}N-TOCSY-HSQC and ^{15}N-NOESY-HSQC); and 60 × 200 × 1024 complex points in the ^{13}C, ^1H, and ^1H dimensions (HCCH-COSY, HCCH-TOCSY, and ^{13}C-NOESY-HSQC). Three-dimensional ^{15}N-separated and ^{13}C-separated NOESY spectra were acquired with a mixing time of 130 and 110 ms, respectively. The 3D (HN)CO(CO)NH experiment (*9*) was used to measure $^3J_{C'C'}$ coupling in uniformly ^{13}C,^{15}N-labeled N116. To identify the slowly exchanging amides, the ^{15}N-labeled sample (either N116 or Δ81Δ) was lyophilized and then dissolved in D_2O (99.96% D), and the experiments for ^1H-^2D exchange were performed at 295 K.

NMR data were processed using NMRPipe and NMRDraw (*10*) and then assigned with Sparky 3 (*11*). Unambiguous assignments for signals from $^1H^N$, ^{15}N, $^{13}C^\alpha$, $^{13}C^\beta$, and $^{13}C'$ nuclei were obtained from 3D CBCANH, CBCA(CO)NH, HNCA, HN(CO)CA, HNCO, and HN(CA)CO experiments on a uniformly ^{13}C,^{15}N-labeled sample of N116 or Δ81Δ. These assignments were extended to side-chain sites using 3D CBCA(CO)NH, HBHA(CBCACO)NH, HCCH-TOCSY, and ^{15}N-separated TOCSY spectra.

Distance Restraints from Paramagnetic Relaxation Enhancement. In the case of the spin-labeled protein sample, the ^1H,^{15}N-HSQC spectra of solutions containing 0.2 mM ^{15}N-labeled N116 A7C* or N116 A11C* in the absence or presence of the reducing reagent (sodium ascorbate) were recorded at 298 K and at a ^1H frequency of 600.13 MHz. Briefly, after acquiring an HSQC of the spin-labeled sample in its oxidized state, a 5-fold molar excess of sodium ascorbate was added from a concentrated stock to reduce the spin label without significantly altering the sample volume and pH. Samples were placed in the magnet at 298 K for at least 1 h to ensure complete reduction of the spin label, and then a second HSQC spectrum was acquired with all of the same parameters. Control spectra were acquired using a solution containing 0.2 mM ^{15}N-labeled N116 and 0.2 mM unlabeled N116 mutant (A7C* or A11C*) in the absence or presence of sodium ascorbate. Any intermolecular interactions and/or aggregation would be detected as significant reductions in the intensity ratios in this control experiment.

The PBEs (paramagnetic broadening effects) by spin probes were converted into distances using eqs 3−5 presented by Battiste and Wagner (*12*). The distances (d_R) calculated from $R2^{sp}$ and τ_c (about 7 ns) were divided into three classes of restraints for structure modeling. Cross-peaks undetectable in the oxidized HSQC spectrum were restrained with no lower bound and an upper bound of a target distance estimated from the noise plus 4 Å. In fact, the free electron of the nitroxide is typically 8−10 Å from the nearest backbone amide (including its own residue) since it is extended into solvent. In practical use, the amide resonances broadened beyond detection actually represent a 5 Å range from 9 to 14 Å. Detectable peaks (in the oxidized HSQC spectrum) with an intensity ratio of $I_{ox}/I_{red} < 0.85$ were restrained with the calculated distances ± 4 Å bounds. Peaks with an intensity ratio of $I_{ox}/I_{red} > 0.90$ were restrained with no upper bound and a lower bound of a target distance calculated from an intensity of 0.90 minus 4 Å.

Structure Calculations. The 11 residues (AAALEHHHHHH) at the C-terminus as an artifact from the vector were not included in structure calculation. Ranges of NOE distance constraints were defined according to their intensities with a lower limit of 1.8 Å and upper limits that were classified into strong (3.0 Å), medium (4.0 Å), and weak (5.0 Å). The lower limit of 1.8 Å was imposed only implicitly by the van der Waals repulsion force. Backbone dihedral angle restraints (phi and psi) were obtained from an analysis of $^{1}H^{\alpha}$, $^{13}C^{\alpha}$, $^{13}C^{\beta}$, $^{13}C'$, and ^{15}N chemical shifts using the program TALOS (*13*).

For N116, structure calculations were carried out using the default settings of Xplor-NIH 2.18 (*14*) and starting from an extended structure of N116 A7C* and A11C*, a double-mutation version of N116. In the initial rounds of calculation, only unambiguous NOEs of sequential and medium-range, dihedral angle restraints, and $^{3}J_{C'C'}$ coupling restraints were used; the long-range NOEs and PBEs, and the hydrogen bonds were then introduced into calculation steps; at the final stage, a set of 400 structures was generated. For Δ81Δ, 300 structures were generated using the default settings of CNS 1.1 (*15*). The final ensemble of each contained 20 lowest-energy structures with no distance restraint violation >0.5 Å and no dihedral angle restraint violation $>5°$. The calculated structures were analyzed and visualized by the programs MOLMOL (*16*) and PyMOL (DeLano Scientific).

NMR Titration Experiments. For NMR interaction studies, ^{1}H,^{15}N-HSQC spectra were recorded at 298 K along the stepwise titration of N116 by a randomly chosen but A/T-rich 20-bp duplex DNA (5′-CATTTATTTATTTATTTAAG-3′/5′-CTTAAATAAATAAATAAATG-3′; 10 mM stock solution) with a sample dilution of less than 10%. ^{15}N-labeled N116 sample concentration was set to 0.1 mM, and the molar ratios of DNA to protein were as follows: 1/10, 1/3, 1/1, 2/1, 4/1, 7/1, and 10/1. Titration experiments were performed in a 20 mM MES (2-(*N*-morpholino)ethanesulfonic acid) buffer with 140 mM NaCl, 5 mM $MgCl_2$, 1 mM EDTA, and 10% (v/v) D_2O at a controlled pH 6.0. The ^{1}H,^{15}N-HSQC of this protein free of DNA was also recorded as a control spectrum. Combined ^{1}H and ^{15}N chemical shift perturbation (CSP) was calculated using eq 1 presented by Liu et al. (*17*).

Yeast Strains and Culture Conditions. Yeast strain BY4741 (MAT*a his3*Δ1 *leu2*Δ0 *met15*Δ0 *ura3*Δ0) and its derived deletion strains (*ymr074c*Δ and *yca1*Δ) were purchased from EUROSCARF. The DNA fragments encoding the full-length and the helix α-truncated Ymr074cP were amplified by PCR and cloned into the galactose-inducible expression vector pESC-URA (Stratagene) using the BamH I and *Sal* I cloning sites to give plasmids pESC/*YMR074c* and pESC/*ymr074c*$^{\Delta\alpha1}$, respectively. pESC-URA, pESC/*YMR074c*, and pESC/*ymr074c*$^{\Delta\alpha1}$ were transformed into the yeast strain *ymr074c*Δ, giving the corresponding yeast strains EUY0, EUY1, and EUY2, respectively. Additionally, pESC-URA and pESC/*YMR074c* were transformed into the yeast strain *yca1*Δ, giving the yeast strains EUY3 and EUY4, respectively.

Yeast growth conditions and induction of expression were reported by Madeo et al. (*18*). Briefly, the *YMR074c*- or *ymr074c*$^{\Delta\alpha1}$-overexpressing strains and the corresponding controls were grown on SCD medium without uracil (pESC-URA). When cultures reached an OD_{600} of 0.3 (10^7 cells mL^{-1}), they were centrifuged and resuspended with 1 volume of SC containing the same amino acids but 2% galactose instead of 2% glucose. For stimulation of yeast apoptosis, H_2O_2 was added to a final concentration of 0.8 mM just after the galactose shift. For inhibition of apoptosis, zVAD-fmk (a 20 mM stock in DMSO) was added to a final concentration of 20 μM at the same time that apoptosis is induced. Cultures were then shaken at 30 °C for 20 h. It was particularly important that all strains in an experiment had almost identical cell density before and after the galactose shift.

Western Blotting. Approximately 5 mg of yeast cells was collected from a liquid culture, resuspended in 200 μL of 100 mM NaOH, and incubated for 5 min at room temperature. The sample was centrifuged, resuspended in 50 μL of SDS−PAGE

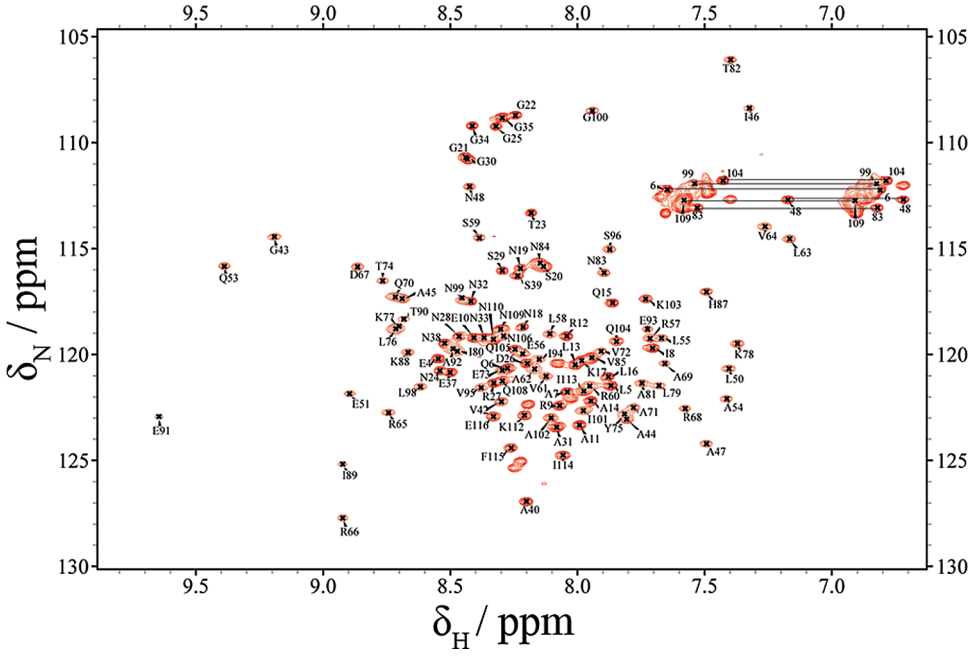

FIGURE 1: Two-dimensional ^{1}H,^{15}N-HSQC spectrum of N116 (residues 1−116 of Ymr074cP), annotated with residue assignments. The side-chain amide resonances of asparagines and glutamines are also labeled and indicated by the horizontal lines.

sample buffer, and boiled for 5 min as reported (*19*). Sample proteins were separated on a SDS−PAGE and electroblotted to a nitrocellulose membrane (Amersham Biosciences). Blots were probed with mouse monoclonal antibody against the c-myc epitope (Sigma).

Test for Apoptotic Markers. DAPI staining (*20*) and TUNEL (*21*) were performed as reported.

In Vivo Staining of Caspase-Like Activity. Caspase activity was measured by using a CaspACE FITC-VAD-fmk in situ marker from Promega according to the manufacturer's instructions. Briefly, 5×10^6 yeast cells were stained with 10 μM FITC-VAD-fmk at room temperature in the dark for 30 min. Cells were washed three times and resuspended in 500 μL of PBS buffer. FACS analysis of cells was performed with excitation of 488 nm and emission of 525−550 nm.

RESULTS

NMR Structural Determination. Initially, the full-length Ymr074cP (145 aa) was expressed as a recombinant protein in *E. coli*. The ^{1}H,^{15}N-HSQC spectrum of this protein had a large number of dispersed backbone amide resonances, characteristic of a folded structure, as well as many severely overlapped backbone amide resonances in the central random coil region, indicative of an unfolded polypeptide (data not shown). To explore these regions, three smaller constructs, designated as N116 (residues 1−116 lacking the C-terminal 29 residues), C110 (lacking the N-terminal 35 residues), and Δ81Δ (residues 36−116 lacking both of them), were subsequently prepared. We found that the fragment corresponding to the C-terminal 29 residues of Ymr074cP was unstructured in solution (data not shown), and therefore, it was not considered in our further structural studies.

The structure of recombinant N116 was determined by multidimensional heteronuclear NMR spectroscopy. Figure 1 shows a ^{1}H,^{15}N-HSQC spectrum of N116. All backbone amide resonances except Asp^2, Gly^{36}, Phe^{49}, Thr^{86}, and Ser^{107} were assigned. Of the 107 identified backbone amide sites, Asn^{19} and Ser^{111} or Ala^{31} and Ile^{97} are overlapped. There is a good dispersion of the backbone amide proton and nitrogen resonances of the core moiety (Gly^{43}-Gln^{105}). The ^{1}H^N chemical shift dispersion between Leu^{63} and Glu^{91} is 2.48 ppm, indicating that the polypeptide possesses a well-defined tertiary fold. In contrast, backbone amide resonances from the N-terminal one-third (Glu^4-Val^{42}) and the C-terminal tail (Asn^{106}-Glu^{116}) are more intense and have a much smaller ^{1}H^N chemical shift dispersion (0.85 ppm) than those from the core moiety; such features are associated with a lack of tertiary structure.

The elements of secondary structure were inferred using ^{1}H$^\alpha$, ^{13}C$^\alpha$, ^{13}C$^\beta$, and ^{13}C′ chemical shifts (Supporting Information Figure S1) and sequential and medium-range NOE connectivities (Supporting Information Figure S2) obtained from the 3D ^{15}N-separated and ^{13}C-separated NOESY spectra. N116 comprises five α-helical regions (residues 3−15, 43−48, 52−64, 66−83, and 90−105). The medium-range NOE connections observed for the region spanning residues 3−15 indicate that the N-terminal portion possesses helical secondary structure, rather than the random coil features expected from a preliminary examination of the ^{1}H,^{15}N-HSQC spectrum of N116 (Figure 1). These results suggest that the N-terminal portion of N116 should be flexible but have the capacity to form a helix.

All of the 169 long-range NOEs were observed only within the core moiety without exception, indicative of the formation of a well-folded structure in this region. The nitroxide side chain, introduced by coupling to the mutant cysteine residue at position 7 or 11 (Supporting Information Figure S3), was used as a probe of long-range interactions. Significant transient interactions were probed between the N-terminal helical portion and the core moiety plus several residues in the C-terminal tail (Supporting Information Figure S4A and C). Under physiological conditions or the conditions for NMR experiments, such transient interactions may take place via electrostatic interactions between the negatively charged side chains of Asp^2, Glu^4, and Glu^{10} and the positively charged side chains of Lys^{77} and Lys^{78}. The effects arising from intermolecular interactions and/or aggregation are very weak and can be neglected (Figure S4B and D, Supporting Information). Size-distribution analysis of this protein by sedimentation velocity ultracentrifugation has also indicated that N116 exists as a monomer (data not shown).

Because of the r^{-6} averaging effects, caused by the flexibility of the N-terminal helix and that of the nitroxide side chain, the distance restraint d_R calculated from $R2^{sp}$ and τ_c (about 7 ns) is interpreted as a r^{-6}-weighted, time and ensemble-averaged distance between the spin label and an amide proton (*6*). The spirit of a semiquantitative restraint is used in the structural interpretation of the PBE data, but with relatively loose (±4 Å) bounds. On the basis of the 142 (72 for N116 A7C* and 70 for N116 A11C*) such loose distance restraints together with the 1662 conventional restraints (summarized in Table 1; 1483 NOE-derived distance

Table 1: NMR Restraint and Structure Statistics for the Final Ensemble

	N116	Δ81Δ
Distance Restraints		
unambiguous NOE	1483	1279
intraresidue ($\|i-j\|=0$)	439	361
sequential ($\|i-j\|=1$)	418	359
medium-range ($1<\|i-j\|<5$)	457	391
long-range ($\|i-j\|\geq 5$)	169	168
hydrogen bonds	29	30
PBE	142	/
Dihedral Angle Restraints		
Phi	54	44
Psi	53	44
^3J coupling restraints	14	/
rmsd from Restraints and Idealized Geometry		
distances (Å)	0.015 ± 0.002	0.006 ± 0.001
dihedral angles (deg)	0.36 ± 0.06	0.18 ± 0.02
^3J couplings (Hz)	0.26 ± 0.08	/
bonds (Å)	0.0011 ± 0.0001	0.0031 ± 0.0001
angles (deg)	0.40 ± 0.01	0.32 ± 0.01
impropers (deg)	0.28 ± 0.01	0.19 ± 0.01
Average Pairwise rmsd to Mean Structure		
all heavy atoms (Å)	2.18[a], 1.11[b], 1.00[c]	1.02[d]
backbone atoms N, C$^\alpha$, C′ (Å)	1.71[a], 0.40[b], 0.46[c]	0.52[d]
Ramachandran Plot		
most-favored region (%)	83.9[a]	85.2[d]
additionally allowed region (%)	12.5[a]	12.5[d]

[a] Calculations or statistics were made for Pro3-Glnl5 plus Gly43-Glnl05. [b] Calculations or statistics were made for Pro3-Glnl5. [c] Calculations or statistics were made for Gly43-Gln 105 (N116). [d] Calculations or statistics were made for Gly43-Gln 105 (Δ81Δ).

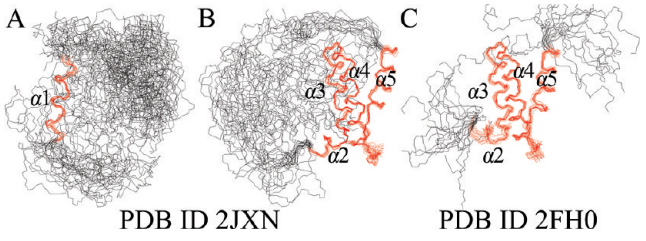

FIGURE 2: Superposition of backbone traces from the final ensemble of 20 solution structures of N116 (PDB ID 2JXN) using (A) Pro^3-Gln^{15} and (B) Gly^{43}-Gln^{105}, and from the final ensemble of 20 solution structures of Δ81Δ (PDB ID 2FH0) using (C) Gly^{43}-Gln^{105}. For comparison, the elements of secondary structure are indicated in each plot.

restraints, 29 hydrogen bonds, 107 phi and psi backbone dihedral angle restraints, and 14 $^3J_{C'C'}$ coupling restraints), an ensemble of compatible structures was generated.

Description of the Ensemble of N116 Structures. Table 1 lists the structural statistics for the 20 representative conformers deposited into the Protein Data Bank (PDB ID 2JXN). A superposition of the backbone traces of the final ensemble is shown in Figure 2A and B. The average backbone rmsd (root-mean-square deviation) is 4.14 Å for Pro^3-Gln^{105}. In sharp contrast to the full protein, the structure for the individual structural region converges well. The average backbone RMSDs for the core moiety (Gly^{43}-Gln^{105}) and the N-terminal helix (Pro^3-Gln^{15}) are 0.46 Å and 0.40 Å, respectively. A PROCHECK analysis of the 20 conformers indicated that 96.4% of the well-defined residues (Pro^3-Gln^{15} plus Gly^{43}-Gln^{105}) lie in the most favored region and the additionally allowed region of the Ramachandran plot. Although the structured N-terminal helix and the folded core were well restrained by the NOE-derived distance restraints, the overall structure of N116 is calculated from a number of imprecise, average restraints to backbone protons. We conclude that the best representation of these structures in Euclidean space should not be a single average structure but rather a set of superimposed backbone traces.

A cartoon representation of the structures (Figure 3B; PDB ID 2JXN) clearly reveals that the overall structure of N116 comprises two structurally distinct regions: N116-n representing a structured α-helix (α1, Pro^3-Gln^{15}) and N116-c (Gly^{43}-Gln^{105}), a helical core. These two regions are tethered by a 27-residue, highly disordered linker (Leu^{16}-Val^{42}). Analysis of the amino acid components of this linker revealed that an abundant content (27%) of glycine existed in the linker. The helical core in Ymr074cP N116 adopts an extended triple-helix bundle fold made up of four α-helices, α2−α5. One of the remarkable features of this fold is that three helices (α3−α5) form a right-handed-twist bundle, as observed in the C-terminal domain of the DNA helicase RuvA subunit (*22*), even though the sequences of these two protein families do not show a significant homologue. Within the helical core, α2 (Gly^{43}-Asn^{48}) and α3 (Pro^{52}-Val^{64}) are joined together by a type-I turn (Phe^{49}-Glu^{51}); α4 (Arg^{66}-Asn^{83}) and α5 (Thr^{90}-Gln^{105}) are connected by a 6-residue linker (Asn^{84}-Ile^{89}); notably, the long helical region between Pro^{52} and Asn^{83} is broken into two portions (α3 and α4) at Arg^{65}. No β-sheet is observed in both structural regions.

The region spanning residues 2−17 has a unique electrostatic potential character with the negatively charged side chains of Asp^2, Glu^4, and Glu^{10} distributed on one side and those positively charged side chains of Arg^9, Arg^{12}, and Lys^{17} on the opposite side of the surface (Figure S4F, Supporting Information). The structure of N116-c is stabilized by hydrophobic interactions, and the amino acid residues via their side chains involved in these hydrophobic interactions are Leu^{50}, Leu^{58}, Val^{61}, Ala^{69}, Val^{72}, Leu^{76}, Ile^{89}, Ile^{94}, Ile^{97}, Leu^{98}, and Ile^{101} (Figure 4C and D). The side chains of these residues may form a hydrophobic core, and those of Leu^{58}, Val^{72}, and Ile^{94} play an important role in forming and stabilizing the hydrophobic core. Besides the residues occurring in the helical regions of the triple-helix bundle, Leu^{50} (in the type I turn) and Ile^{89} (at the end of the linker 2) are also involved in the hydrophobic interactions (Figure 4D).

Structural Comparisons. Figure 3A, a multiple sequence alignment of 10 selected members of the PDCD5 family, clearly indicates that the amino acid residues corresponding to the secondary structures (α1−α5) of Ymr074cP N116 are well conserved during the evolution from yeast to man. The solution structure of Ymr074cP N116 determined here is closely related to those of human PDCD5 and *Methanobacterium thermoautotrophicum* MTH1615 (Figure 3B). Similar to Ymr074cP N116, hPDCD5 also contains a structured N-terminal α-helix (Asp^3-Ala^{19}, PDB ID 1YYB) (*23*) and a helical core (Asp^{26}-Ser^{100}, PDB ID 2CRU). The residues Asp^3-Ala^{19} of hPDCD5 are 53% identical to those of Ymr074cP N116 (Figure 3A). Most notably, the flexible linker (Lys^{20}-Gly^{25}) of hPDCD5 is much shorter than that (Leu^{16}-Val^{42}) of Ymr074cP N116; the amino acid sequence corresponding to Asp^{26}-Gln^{46} of hPDCD5, however, tends to form a long helical secondary structure during vertebrate evolution. Although it was reported that the fragment corresponding to the N-terminal 31 residues of MTH1615 was unstructured in solution and truncated before the determination of the structure of the core (*24*), we strongly suggest that the residues Asp^3-Gln^{17} of MTH1615 have the potential to form a helical structure because they are evolutionarily conserved and 47% identical to those of hPDCD5 (Figure 3A). In addition, there is also a helical core (Lys^{40}−Ala^{100}, PDB ID 1EIJ) in MTH1615.

As Ymr074cP N116, both the helical cores of MTH1615 and hPDCD5 are also stabilized by hydrophobic interactions (Figure 4). The residues (except Leu^{44} and Val^{47} of hPDCD5) involved in these hydrophobic interactions are well conserved across the structures; Leu^{56}, Ile^{70}, and Leu^{92} of MTH1615, and Leu^{48}, Leu^{56}, Leu^{74}, and Leu^{92} of hPDCD5 are the key residues to form and stabilize their respective hydrophobic cores. By contrast with Leu^{50} or Ile^{89} of Ymr074cP N116, neither Leu^{48} of MTH1615 (Figure 4B, indicated in gray) nor Val^{87} of hPDCD5 (Figure 4F, indicated in gray) is involved in the hydrophobic interactions mentioned above.

A description of structural similarities found in these helical cores using the combinatorial extension method (*25*) is presented in Table 2. Over a selection of residues corresponding to the helical core of Ymr074cP N116, the backbone C^α rmsd values are 2.0 Å (Z-score: 4.7) between Ymr074cP N116 (PDB ID 2JXN) and hPDCD5 (PDB ID 2CRU), and 3.3 Å (Z-score: 4.4) between Ymr074cP N116 and MTH1615 (PDB ID 1EIJ). This structural homologue was used to construct an alignment of the amino acid sequences (data not shown), which shows that the helical core of Ymr074cP N116 is 31% identical to that of hPDCD5 and 28% identical to that of MTH1615.

Overall, the polypeptide-chain routes of triple-helix bundles (α3−α5) are very similar between Ymr074cP N116 and hPDCD5. However, the significant differences between the two structures of Ymr074cP N116 and hPDCD5 are that the second helix (α2, Gly^{43}-Asn^{48}) of Ymr074cP N116 is much shorter than that of hPDCD5 (Figure 3) and that in hPDCD5 the second helix

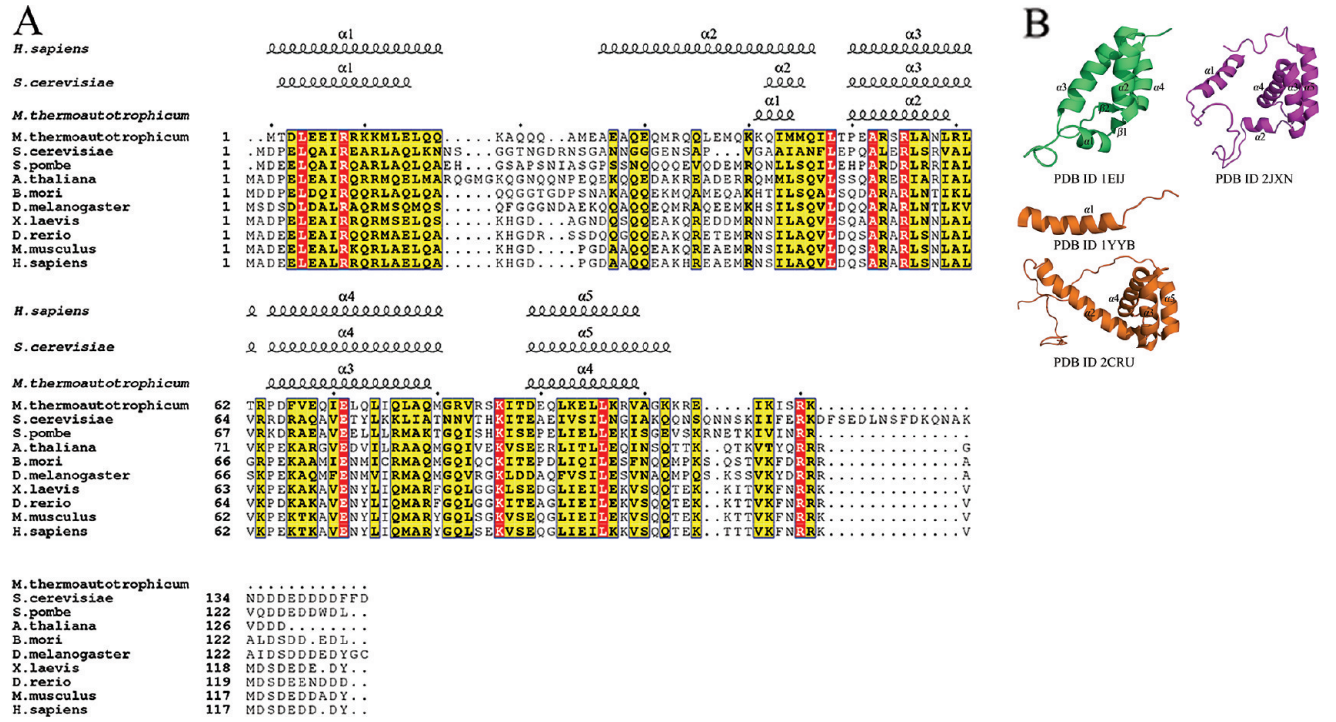

FIGURE 3: (A) An ESPript (*44*) output of multiple sequence alignment of 10 full-length PDCD5-related proteins aligned with CLUSTAL W2 (*45*). Sequences are divided into three groups according to similarity. Residues strictly conserved across sequences are boxed and indicated by bold letters in red background, residues well conserved according to a Risler matrix are also boxed and indicated by bold letters in yellow background, and the remainders are in regular black. For comparison, the elements of secondary structure are indicated corresponding to the amino acid sequences of MTH1615, Ymr074cP N116, and hPDCD5, respectively. (B) A ribbon show of the representative NMR structures of MTH1615 (PDB ID 1EIJ), Ymr074cP N116 (PDB ID 2JXN), and hPDCD5 (PDB ID 1YYB and 2CRU). The elements of secondary structure are also labeled in each structure. For comparison, only one of the conformations in the ensemble of Ymr074 cP N116 is shown here.

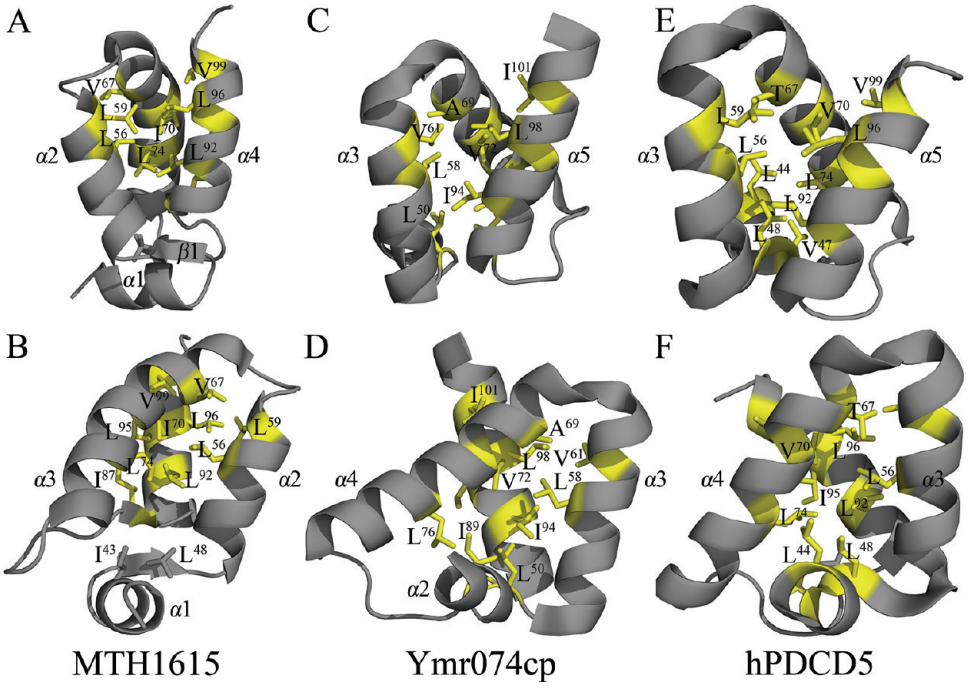

FIGURE 4: Hydrophobic interactions in the helical cores of MTH1615, Ymr074cP N116, and hPDCD5. The residues involved in these hydrophobic interactions are labeled and indicated in yellow.

(α2, Asp[26]-Gln[46]) and the following turn (Val[47]-Asp[49]) are drawn to the triple-helix bundle because of the hydrophobic interactions of the side chains of Leu[44], Val[47], Leu[48], and Leu[74] (Figure 4E and F). A similar fold of helical core is also found between the two structures of Ymr074cP N116 and MTH1615; on the basis of the structure alignment with 2JXN or 2CRU, we found that there is an insert of four amino acid residues (Met[44], Met[45], Gln[46], and Ile[47]) in the structure of MTH1615 (data not shown), which in return affects the polypeptide-chain route of the first helix (α1, Lys[40]-Met[45]) and results in the formation of a short β-sheet (β1, Ile[47]-Thr[49]) (Figure 3B). Because of the insert of these amino acid residues, neither Ile[43] nor Leu[48] is involved in

Table 2: Root-Mean-Square Deviations between the Backbone C^{α} Coordinates of a Range of Structures (in Å)[a]

	2FH0	2CRU	1EIJ
2JXN	0.9	2.0	3.3
2FH0		1.9	3.4
2CRU			4.0

[a] The rmsd was determined for 61 residues equivalent to Ala^{44}-Gln^{104} of *S. cerevisiae* Ymr074cP. PDB codes 2JXN and 2FH0; *S. cerevisiae* Ymr074 cp. PDB code 2CRU; human PDCD5. PDB code 1EIJ; *M. thermoautotrophicum* MTH1615.

the hydrophobic interactions by which the helical core of MTH1615 is stabilized (Figure 4A and B). Taken together, these results clearly indicate that Ymr074cP N116 is more structurally related to hPDCD5 than to MTH1615 in their shared domains.

Chemical Shift Perturbations by Duplex DNA. A comparison of the electrostatic potential surfaces of MTH1615, Ymr074cP N116, and hPDCD5 revealed an evolutionarily conserved basic cleft. The basic clefts are constituted by Arg^{55}, Arg^{63}, Lys^{93}, and Lys^{97} of MTH1615, Arg^{57}, Arg^{60}, Arg^{65}, and Arg^{68} of Ymr074cP N116, and Arg^{55}, Lys^{63}, Lys^{66}, and Lys^{97} of hPDCD5 (Figure 5). Notably, the residue corresponding to Arg^{57} of Ymr074cP N116 is strictly conserved during the evolution of this kind of protein (Figure 3A). It was reported that MTH1615 can interact nonspecifically with a randomly chosen 20-bp duplex DNA in an EMSA (electrophoretic mobility shift assays) and that the basic cleft mentioned above (Figure 5A) was predicted as the DNA-binding interface on the protein (*24*). However, the real molecular function of such a conserved basic cleft is unknown.

Titration of ^{15}N-labeled Ymr074cP N116 with progressive amounts of unlabeled 20-bp duplex DNA was performed by monitoring changes in ^{1}H,^{15}N-HSQC spectra. The NMR titration experiment data are summarized in Supporting Information (Figure S5). We have noticed the DNA-to-protein molar ratio of 4/1 at which the resonances of His^{87} and Lys^{88} show strong CSP. From this point on, both His^{87} and Thr^{82} exhibit continuous CSP, and Lys^{88} will be badly overlapped with Asn^{38}. However, the other residues including the expected basic residues such as Arg^{57}, Arg^{60}, Arg^{65}, and Arg^{68} have very small CSP during the titration. Because the resonance of Thr^{86} is not assigned in the ^{1}H,^{15}N-HSQC spectra, it is not clear whether the polar residue adjacent to His^{87} is perturbed. Figure 3A clearly indicates that His^{87} is specific for the PDCD5 homologues from *S. cerevisiae* and *Schizosaccharomyces pombe*, whereas Lys^{88} is strictly conserved during the evolution of this kind of protein. In addition, Ymr074cP N116 shows very weak binding affinity to a randomly chosen duplex DNA in an EMSA (data not shown). If the DNA-binding property of Ymr074cP N116 is true, His^{87} or/and Lys^{88} might form a potential DNA-binding interface on this protein rather than the conserved basic cleft predicted before.

YMR074c Overexpression Promotes H_2O_2-Induced Yeast Apoptosis Mediated in Part by Yca1. Over the past decade, yeast has been used successfully as a model system for studying the molecular mechanisms of apoptotic cell death (*18*, *20*, *26*−*28*). To study the potential role of Ymr074cP in yeast apoptosis, a plasmid encoding *YMR074c* C-terminally tagged with a myc epitope under the control of a *GAL1* promoter was used to induce the overexpression of Ymr074cP protein in yeast. The galactose-inducible expression of the Ymr074cP protein was analyzed by immunoblotting. A prominent band of about 21 kD

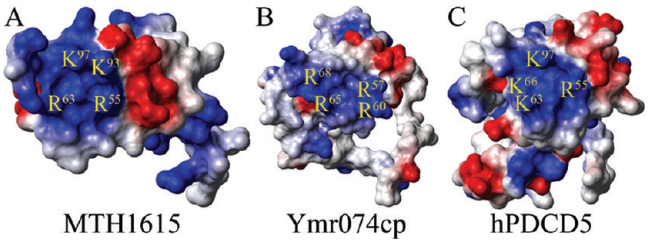

FIGURE 5: Conserved basic clefts on the electrostatic potential surfaces of (A) MTH1615, (B) Ymr074cP N116, and (C) hPDCD5. The residues constituting their respective basic clefts are labeled and indicated in blue.

(theoretical molecular weight: 18.0 kD), which was absent in the corresponding vector control, was detected with the myc-specific antibody after induction for 20 h with galactose media in *YMR074c* overexpressor (Figure 6A).

H_2O_2 has been shown to cause apoptosis in mammalian cells and yeast (*18*, *29*), and was used to induce apoptosis in yeast in this study. In order to monitor the activation of endogenous caspase-like proteases in response to the induction of apoptosis, yeast cells were incubated in vivo with FITC-labeled VAD-fmk as reported by Madeo et al. (*18*). *YMR074c* overexpressor and the corresponding vector control were compared (both in *ymr074cΔ* background), without further treatment or after stimulation with 0.8 mM H_2O_2. No caspase activation was observed in either culture of the untreated cells (Figure 6B, lane 1). In sharp contrast, after treatment with 0.8 mM H_2O_2, more than 50% *YRM074c* overproducers and about 30% control cells showed FITC-VAD-fmk positive (Figure 6B, lane 2). The percentage of FITC-VAD-fmk positive cells significantly increased, by as much as 25%. However, disruption of wild-type gene *YMR074c* had little effect on H_2O_2-induced apoptosis in yeast (data not shown). When a pan-caspase inhibitor (zVAD-fmk) was added before the addition of H_2O_2, no apparent caspase activity was observed in either H_2O_2-treated culture (Figure 6B, lane 3). Taken together, these results clearly demonstrate that hydrogen peroxide treatment induces apoptosis together with a caspase-like activity, that the pan-caspase inhibitor zVAD-fmk can inhibit the caspase-like activity in yeast, and that *YMR074c* overexpression alone does not trigger but rather significantly promotes H_2O_2-induced apoptosis in yeast.

S. cerevisiae metacaspase Yca1 demonstrates enzymatic peptidase activity analogous to mammalian caspase activity and is inhibited in the presence of zVAD-fmk (*18*). In addition, Yca1 has secondary substrate specificity directed at arginine/lysine motifs (*30*). The programmed cell death events observed in *S. cerevisiae*, due to external stimuli as well as internal signals, were often dependent on the cysteine protease activity of metacaspase Yca1; in other cases, cell death occurred in the absence of this activity (*18*, *31*−*34*).

To investigate the relationship between Ymr074cP and *S. cerevisiae* metacaspase Yca1 during yeast oxidative stress, *YMR074c* overexpressor (Figure 6A, lane 5) and the corresponding vector control (both in *yca1Δ* background) were constructed and treated with H_2O_2 as well. The metacaspase-dependent apoptosis in yeast upon H_2O_2 treatment has been demonstrated by Madeo et al. (*18*). In contrast, apoptotic cell death upon H_2O_2 treatment, as evidenced by caspase activation and DNA fragmentation, was also observed in the *yca1Δ* background (Figure 6B and C), indicating that H_2O_2 also induces metacaspase Yca1-independent apoptosis in yeast. The recent observation

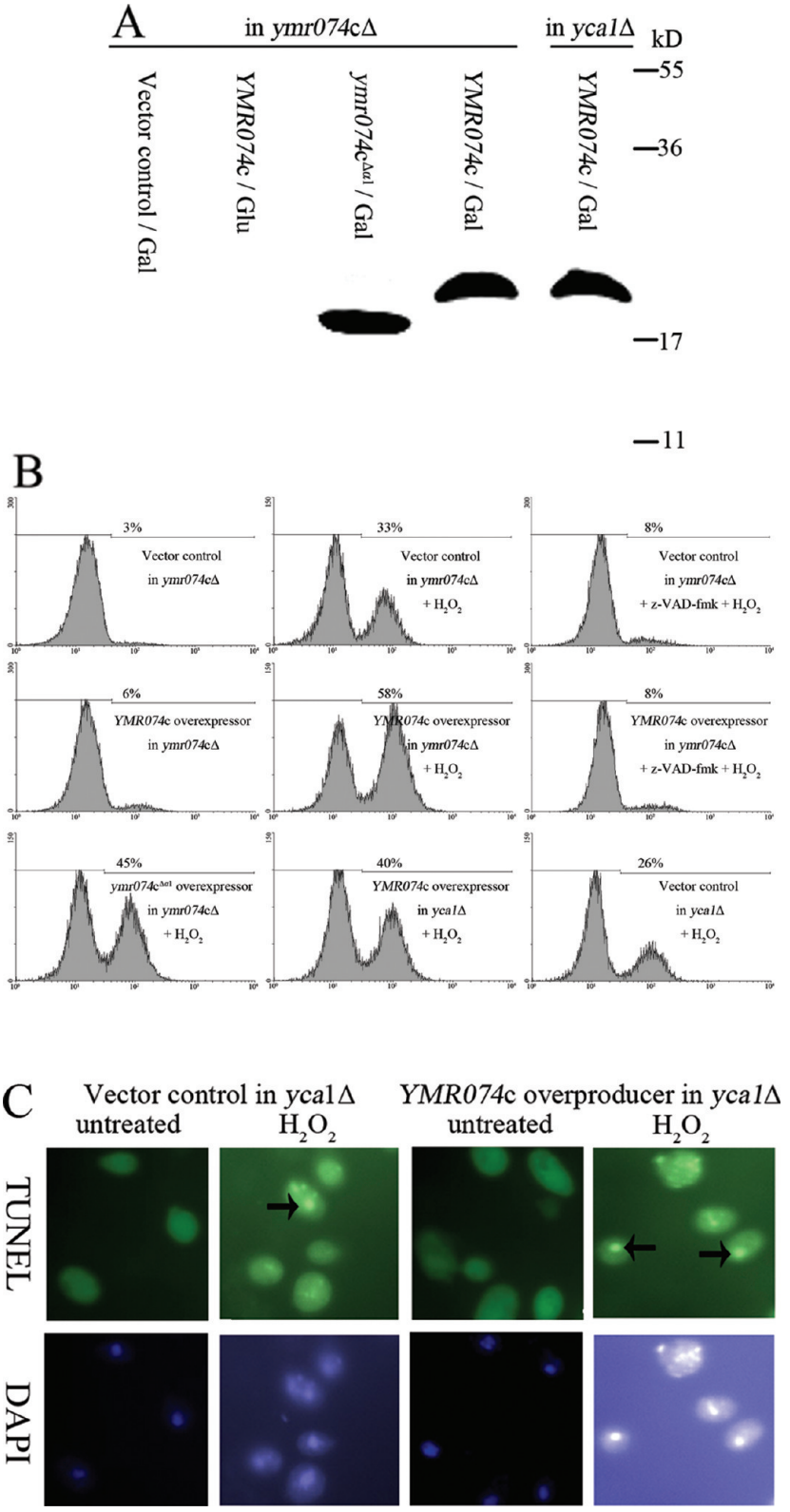

FIGURE 6: (A) Yeast extracts of plasmid-encoded C-terminally myc-tagged Ymr074cP, Ymr074cP$^{\Delta\alpha1}$, and the corresponding vector control grown in either glucose media or induced with galactose media for 20 h were immunoblotted and probed with antimyc antibody. (B) *YMR074c* overproducers, *YMR074c* overproducers in a y*ca1*Δ background, *ymr074c*$^{\Delta\alpha1}$ overproducers, and vector control, grown on galactose media to a certain cell density and treated for 20 h with 0.8 mM H_2O_2 or treated for 20 h with 0.8 mM H_2O_2 plus 20 μM caspase inhibitor zVAD-fmk or untreated, were labeled for active caspase in vivo with FITC-VAD-fmk and analyzed by flow cytometry. (C) TUNEL and DAPI staining of *YMR074c* overproducers and vector control (both in y*ca1*Δ background) treated for 20 h with 0.8 mM H_2O_2 or untreated. The arrows indicate TUNEL positive cells.

that yeast Esp1 also functions as caspase-like protease upstream mitochondria and is responsible for the cleavage of yeast Mcd1 during the H_2O_2-induced apoptosis (*27*) favors our results. Furthermore, we demonstrate that *YMR074c* overexpression promotes apoptosis in yeast in response to H_2O_2 treatment, not only by Yca1-dependent (40% for *YMR074c* overproducers

in *yca1*Δ and 58% for *YMR074*c overproducers in *ymr074*cΔ, both treated with H_2O_2) but also by Yca1-independent (40% for *YMR074*c overexpressors and 26% for control cells, both in *yca1*Δ and treated with H_2O_2) apoptotic pathways.

Structural Integrity of Ymr074cP Is Important for Its Functional Regulation. Overexpression of the α1-truncated mutant *ymr074*c$^{\Delta\alpha1}$ (residues 17−145 of Ymr074cP) (Figure 6A, lane 3) in yeast showed a reduced percentage of cells with caspase activation upon H_2O_2 treatment, compared with that in overexpression of wild-type *YMR074*c (45% for *ymr074*c$^{\Delta\alpha1}$ overexpressors (Figure 6B, lane 1) and 58% for *YMR074*c overexpressors (Figure 6B, lane 2), both treated with 0.8 mM H_2O_2), but more than the percentage (33%) of the corresponding H_2O_2-treated vector control. This demonstrates that deletion of the first helical region (α1) of the Ymr074cP protein greatly attenuates rather than completely eliminates the apoptosis-promoting activity of this protein.

Subsequently, we determined the solution structure of truncated mutant Δ81Δ (residues 36−116) with 1279 NOE distance restraints, 30 hydrogen bonds, and 88 backbone dihedral angle restraints. Table 1 summarized the data of restraint and structure statistics for the final ensemble of 20 NMR structures of Δ81Δ as well. As expected, the helical cores of N116 and Δ81Δ exhibit very similar fold topology. The backbone C^{α} rmsd between these two structures is 0.9 Å (Table 2; Figure 2B and C). This demonstrates that the core of Ymr074cP can fold independently of the mobile N-terminal helical structure and that the topology of the triple-helix bundle is indeed encoded mainly by intrinsic hydrophobic interactions. With all of the data taken together, we conclude that both the N-terminal helical portion and the helical core are important functional regions of the Ymr074cP protein. It means that the structural integrity of this protein is very important for its functional regulation.

DISCUSSION

The hPDCD5 protein has been identified as a novel programmed cell death-promoting molecule in recent years (*1*, *3*, *5*, *35*, *36*). hPDCD5 may exert its apoptosis-promoting activity by modulating Bax translocation to mitochondria, cytochrome *c* release from mitochondria, and caspase 3 activation directly or indirectly (*36*). Yeast lacks obvious orthologues of many key mammalian apoptotic regulators, including the Bcl-2 family proteins, challenging a conserved molecular mechanism by which PDCD5 family proteins regulate yeast and mammalian apoptosis. Yeast was used as a tool to study the regulation of mitochondria-dependent cell death induced by Bcl-2 family proteins, and there are several contradictory results regarding the mode of cell death induced by Bax expression in yeast (*28*, *37*). Recent research indicates that yeast possibly does encode functional/structural equivalents of Bcl-2 family proteins, despite the absence of significant amino acid sequence similarity (*27*, *38*, *39*).

In this study, we demonstrate a promoting role for *YMR074*c overexpression in H_2O_2-induced apoptosis in yeast that is mediated by both Yca1-dependent and Yca1-independent apoptotic pathways, although the mechanisms remain unclear. Our observations favor the possibility that programmed cell death is an important function of metacaspases (*32*, *33*, *40*). There are several reports in favor of a role of metacaspase Yca1 upstream mitochondria (*28*). On the contrary, Yca1 appears to act on downstream mitochondria in hyperosmotic stress-induced apoptosis (*41*). That study showed a partial dependence of caspase activation on cytochrome *c*. So far, no known target substrate of yeast metacaspase Yca1 has been identified. Our results also indicate Yca1-independent caspase activation upon H_2O_2 treatment in yeast. Esp1 is another caspase-like yeast protease implicated in programmed cell death and is conserved in mammals (*27*). This cysteine protease was recently reported to cleave yeast Mcd1, an orthologue of human cohesin Rad21. Although the critical cleavage site in yeast Mcd1 was not identified, a C-terminal cleavage fragment of Mcd1 was reported to translocate to mitochondria and trigger cyt *c*-dependent cell death in yeast.

We also demonstrate that Ymr074cP N116 is a flexibly folded protein, in which an extended triple-helix bundle at the C-terminus is connected to a structured α-helix in the N-terminus by means of a highly flexible linker. The topology of such an extended triple-helix bundle is encoded mainly by hydrophobic interactions. In the present work, we failed to characterize any long-range NOE that connects the N-terminal one-third (residues 1−42) and the other residues (43−116) of N116 by analysis of the NOESY spectra of uniformly ^{13}C,^{15}N-labeled N116. Obviously, the dipolar interaction between protons, with its restriction to distances under 5.5 Å and its high sensitivity to correlation times, is not an ideal probe for identifying transient interactions between mobile chain segments over long distances. The dipolar interaction between a free electron and a proton, however, may be a more suitable probe of the global structures of partially or flexibly folded proteins since the range of this interaction extends over 20 Å. Therefore, the relative positions between the N-terminal helix and the triple-helix bundle were determined by the paramagnetic spin labeling method. The equation used to calculate distance restraint d_R assumes that the distance from the nitrogen atom of the nitroxide to the hydrogen atom of the respective amide is constant and that the correlation time for the electron−proton vector depends on isotropic rotation. However, neither of these two conditions is met in the current application since the whole N-terminal helical region is mobile relative to the helical core. The most significant sources of uncertainty in d_R are as follows (*6*, *12*): (1) d_R is derived from a heterogeneous ensemble of flexibly folded conformations rapidly interconverting. The sixth-power relationship between r and $R2^{sp}$ will result in the calculated d_R being heavily biased in favor of the shortest distances, causing large errors in the estimate of r. (2) Uncertainty in d_R caused by flexibility of the spin-label side chain. However, at the large distances (> 14 Å) detected by the spin probe, the r^{-6} averaging caused by this kind of flexibility is not a major problem. (3) Errors in the use of one correlation time (τ_c about 7 ns) for all electron−proton vectors. But for a measured value of $R2^{sp}$, the estimate of r will be relatively insensitive to small errors in τ_c because of the dependence of distance on the sixth-root of correlation time. (4) Errors in the accuracy with which $R2^{sp}$ has been measured. Consequently, it is impossible to convert the measured values of $R2^{sp}$ into precise distance restraints. However, the spirit of a semiquantitative restraint, but with relatively loose bounds, makes it possible to interpret the PBE data for structural calculations. Clearly, calculated structures will combine structural features that may not necessarily be present simultaneously in any one conformation and will inevitably be more compact than the true ensemble. These major limitations, plus the fact that a flexibly folded protein is most likely to be a heterogeneous ensemble, should be kept in mind in the interpretation of the results of calculated structures. Finally, it makes

more sense to interpret the calculated structures as an ensemble rather than as individual or average structures.

A structural comparison of PDCD5-related proteins indicates that a member of the PDCD5 family of proteins has a significantly evolutionarily conserved triple-helix bundle, which probably mediates similar molecular/cellular functions, and that the structured α-helix in the N-terminus is possibly conserved during evolution at least from yeast to man as well. Furthermore, structural and functional studies also indicate that the helical core of Ymr074cP has the capacity to fold independently of the N-terminal helical structure and serves as a functional entity to promote H_2O_2-induced apoptosis in yeast and that deletion of the N-terminal helical portion greatly attenuates the function of the entire molecule, implying that the N-terminal helical structure might directly or indirectly regulate the apoptosis-promoting activity of the helical core. So far, whether or not such deletion will cause dissociation of some target proteins is still unknown. A previous report of hPDCD5 has also indicated that the N-terminal helical structure of hPDCD5 is an important functional region of the protein (*23*). Besides, the reported studies on hPDCD5 have revealed that the C-terminal region (residues 109−115), a region rich in basic amino acids flanked by hydrophobic residues (Figure 3A), is also crucial for the biological function of hPDCD5 (*35*, *42*, *43*). Therefore, the role of the C-terminal region of Ymr074cP in its biological function will be examined in our further studies.

ACKNOWLEDGMENT

We thank Professor Changlin Tian for his advice on the application of spin probes to structural analysis.

SUPPORTING INFORMATION AVAILABLE

Figures S1 and S2 summarize the data of NMR secondary chemical shifts and sequential and medium-range NOE connections used in the determination of the secondary structures of Ymr074cP N116. Figures S3 and S4 summarize the data on the N116 mutants with spin labels used to obtain the long-range PBE distance restraints. In addition, Figure S5 presents the data of chemical shift perturbations by duplex DNA during the titration. This material is available free of charge via the Internet at http://pubs.acs.org.

REFERENCES

1. Liu, H., Wang, Y., Zhang, Y., Song, Q., Di, C., Chen, G., Tang, J., and Ma, D. (1999) TFAR19, a novel apoptosis-related gene cloned from human leukemia cell line TF-1, could enhance apoptosis of some tumor cells induced by growth factor withdrawal. *Biochem. Biophys. Res. Commun. 254*, 203–210.
2. Xu, M., Cheng, N., Gui, L., Lai, M., Wang, Y., Xia, D., Rui, M., Zhang, Y., and Ma, D. (2004) The 5′-upstream region of human programmed cell death 5 gene contains a highly active TATA-less promoter that is up-regulated by etoposide. *Gene 329*, 39–49.
3. Rui, M., Chen, Y., Zhang, Y., and Ma, D. (2002) Transfer of anti-TFAR19 monoclonal antibody into HeLa cells by in situ electroporation can inhibit the apoptosis. *Life Sci. 71*, 1771–1778.
4. Li, S. J., Yu, J., Zhao, X. F., Jiang, Y., Liu, Z. J., and Yu, X. G. (2007) PDCD5 induces the apoptosis of human prostate cancer cells PC-3M-1E8. *Zhonghua Nan Ke Xue 13*, 979–982.
5. Wang, Y., Li, X., Wang, L., Ding, P., Zhang, Y., Han, W., and Ma, D. (2004) An alternative form of paraptosis-like cell death, triggered by TAJ/TROY and enhanced by PDCD5 overexpression. *J. Cell Sci. 117*, 1525–1532.
6. Gillespie, J. R., and Shortle, D. (1997) Characterization of long-range structure in the denatured state of staphylococcal nuclease. II. Distance restraints from paramagnetic relaxation and calculation of an ensemble of structures. *J. Mol. Biol. 268*, 170–184.
7. Kosen, P. A. (1989) Spin labeling of proteins. *Methods Enzymol. 177*, 86–121.
8. Cavanagh, J., Fairbrother, W. J., Palmer, A. G. (1995) Protein NMR Spectroscopy: Principles and Practice , Academic Press, San Diego, CA.
9. Grzesiek, S., and Bax, A. (1997) A three-dimensional NMR experiment with improved sensitivity for carbonyl-carbonyl J correlation in proteins. *J. Biomol. NMR 9*, 207–211.
10. Delaglio, F., Grzesiek, S., Vuister, G. W., Zhu, G., Pfeifer, J., and Bax, A. (1995) NMRPipe: a multidimensional spectral processing system based on UNIX pipes. *J. Biomol. NMR 6*, 277–293.
11. Goddard, T. D., and Kneller, D. G. (2006) SPARKY 3 , University of California, San Francisco, CA.
12. Battiste, J. L., and Wagner, G. (2000) Utilization of site-directed spin labeling and high-resolution heteronuclear nuclear magnetic resonance for global fold determination of large proteins with limited nuclear overhauser effect data. *Biochemistry 39*, 5355–5365.
13. Cornilescu, G., Delaglio, F., and Bax, A. (1999) Protein backbone angle restraints from searching a database for chemical shift and sequence homology. *J. Biomol. NMR 13*, 289–302.
14. Schwieters, C. D., Kuszewski, J. J., and Clore, G. M. (2006) Using Xplor-NIH for NMR molecular structure determination. *Prog. Nucl. Magn. Reson. Spectrosc. 48*, 47–62.
15. Brunger, A. T., Adams, P. D., Clore, G. M., DeLano, W. L., Gros, P., Grosse-Kunstleve, R. W., Jiang, J. S., Kuszewski, J., Nilges, M., Pannu, N. S., Read, R. J., Rice, L. M., Simonson, T., and Warren, G. L. (1998) Crystallography & NMR system: A new software suite for macromolecular structure determination. *Acta Crystallogr., Sect. D 54*, 905–921.
16. Koradi, R., Billeter, M., and Wuthrich, K. (1996) MOLMOL: a program for display and analysis of macromolecular structures. *J. Mol. Graphics 14* (51−55), 29–32.
17. Liu, Y., Wang, X. Q., Zhang, J. H., Huang, H. D., Ding, B., Wu, J. H., and Shi, Y. Y. (2008) Structural basis and binding properties of the second bromodomain of Brd4 with acetylated histone tails. *Biochemistry 47*, 6403–6417.
18. Madeo, F., Herker, E., Maldener, C., Wissing, S., Lachelt, S., Herlan, M., Fehr, M., Lauber, K., Sigrist, S. J., Wesselborg, S., and Frohlich, K. U. (2002) A caspase-related protease regulates apoptosis in yeast. *Mol. Cell 9*, 911–917.
19. Kushnirov, V. V. (2000) Rapid and reliable protein extraction from yeast. *Yeast 16*, 857–860.
20. Madeo, F., Frohlich, E., and Frohlich, K. U. (1997) A yeast mutant showing diagnostic markers of early and late apoptosis. *J. Cell Biol. 139*, 729–734.
21. Carré, V., and Guilloton, M. (1997) DNA fragmentation attested by TUNEL in *Saccharomyces cerevisiae* subjected to photodynamic treatment. *J. Microbiol. Methods 29*, 185–190.
22. Ariyoshi, M., Nishino, T., Iwasaki, H., Shinagawa, H., and Morikawa, K. (2000) Crystal structure of the holliday junction DNA in complex with a single RuvA tetramer. *Proc. Natl. Acad. Sci. U.S.A. 97*, 8257–8262.
23. Liu, D., Yao, H., Chen, Y., Feng, Y., and Wang, J. (2005) The N-terminal 26-residue fragment of human programmed cell death 5 protein can form a stable alpha helix having unique electrostatic potential character. *Biochem. J. 392*, 47–54.
24. Christendat, D., Yee, A., Dharamsi, A., Kluger, Y., Savchenko, A., Cort, J. R., Booth, V., Mackereth, C. D., Saridakis, V., Ekiel, I., Kozlov, G., Maxwell, K. L., Wu, N., McIntosh, L. P., Gehring, K., Kennedy, M. A., Davidson, A. R., Pai, E. F., Gerstein, M., Edwards, A. M., and Arrowsmith, C. H. (2000) Structural proteomics of an archaeon. *Nat. Struct. Biol. 7*, 903–909.
25. Shindyalov, I. N., and Bourne, P. E. (1998) Protein structure alignment by incremental combinatorial extension (CE) of the optimal path. *Protein Eng. 11*, 739–747.
26. Eisenberg, T., Buttner, S., Kroemer, G., and Madeo, F. (2007) The mitochondrial pathway in yeast apoptosis. *Apoptosis 12*, 1011–1023.
27. Yang, H., Ren, Q., and Zhang, Z. (2008) Cleavage of Mcd1 by caspase-like protease Esp1 promotes apoptosis in budding yeast. *Mol. Biol. Cell 19*, 2127–2134.
28. Pereira, C., Silva, R. D., Saraiva, L., Johansson, B., Sousa, M. J., and Corte-Real, M. (2008) Mitochondria-dependent apoptosis in yeast. *Biochim. Biophys. Acta 1783*, 1286–1302.
29. Madeo, F., Frohlich, E., Ligr, M., Grey, M., Sigrist, S. J., Wolf, D. H., and Frohlich, K. U. (1999) Oxygen stress: a regulator of apoptosis in yeast. *J. Cell Biol. 145*, 757–767.

30. Watanabe, N., and Lam, E. (2005) Two Arabidopsis metacaspases AtMCP1b and AtMCP2b are arginine/lysine-specific cysteine proteases and activate apoptosis-like cell death in yeast. *J. Biol. Chem. 280*, 14691–14699.
31. Qi, H., Li, T. K., Kuo, D., Nur, E. K. A., and Liu, L. F. (2003) Inactivation of Cdc13p triggers MEC1-dependent apoptotic signals in yeast. *J. Biol. Chem. 278*, 15136–15141.
32. Reiter, J., Herker, E., Madeo, F., and Schmitt, M. J. (2005) Viral killer toxins induce caspase-mediated apoptosis in yeast. *J. Cell Biol. 168*, 353–358.
33. Ivanovska, I., and Hardwick, J. M. (2005) Viruses activate a genetically conserved cell death pathway in a unicellular organism. *J. Cell Biol. 170*, 391–399.
34. Guaragnella, N., Pereira, C., Sousa, M. J., Antonacci, L., Passarella, S., Corte-Real, M., Marra, E., and Giannattasio, S. (2006) YCA1 participates in the acetic acid induced yeast programmed cell death also in a manner unrelated to its caspase-like activity. *FEBS Lett. 580*, 6880–6884.
35. Wang, Y., Li, D., Fan, H., Tian, L., Zhong, Y., Zhang, Y., Yuan, L., Jin, C., Yin, C., and Ma, D. (2006) Cellular uptake of exogenous human PDCD5 protein. *J. Biol. Chem. 281*, 24803–24817.
36. Chen, L., Wang, Y., Ma, D., and Chen, Y. (2006) Short interfering RNA against the PDCD5 attenuates cell apoptosis and caspase-3 activity induced by Bax overexpression. *Apoptosis 11*, 101–111.
37. Cheng, W. C., Leach, K. M., and Hardwick, J. M. (2008) Mitochondrial death pathways in yeast and mammalian cells. *Biochim. Biophys. Acta 1783*, 1272–1279.
38. Fannjiang, Y., Cheng, W. C., Lee, S. J., Qi, B., Pevsner, J., McCaffery, J. M., Hill, R. B., Basanez, G., and Hardwick, J. M. (2004) Mitochondrial fission proteins regulate programmed cell death in yeast. *Genes Dev. 18*, 2785–2797.
39. Komatsu, K., Hopkins, K. M., Lieberman, H. B., and Wang, H. (2000) *Schizosaccharomyces pombe* Rad9 contains a BH3-like region and interacts with the anti-apoptotic protein Bcl-2. *FEBS Lett. 481*, 122–126.
40. Suarez, M. F., Filonova, L. H., Smertenko, A., Savenkov, E. I., Clapham, D. H., von Arnold, S., Zhivotovsky, B., and Bozhkov, P. V. (2004) Metacaspase-dependent programmed cell death is essential for plant embryogenesis. *Curr. Biol. 14*, R339–340.
41. Silva, R. D., Sotoca, R., Johansson, B., Ludovico, P., Sansonetty, F., Silva, M. T., Peinado, J. M., and Corte-Real, M. (2005) Hyperosmotic stress induces metacaspase- and mitochondria-dependent apoptosis in *Saccharomyces cerevisiae*. *Mol. Microbiol. 58*, 824–834.
42. Liu, Y., Ling, X., Fan, H., Zhong, Y., Li, D., and Wang, Y. (2007) Determination of binding constant and binding region of programmed cell death 5-heparin by capillary zone electrophoresis. *J. Chromatogr., A 1143*, 284–287.
43. Ling, X., Liu, Y., Fan, H., Zhong, Y., Li, D., and Wang, Y. (2007) Studies on interactions of programmed cell death 5 (PDCD5) and its related peptides with heparin by capillary zone electrophoresis. *Anal. Bioanal. Chem. 387*, 909–916.
44. Gouet, P., Courcelle, E., Stuart, D. I., and Metoz, F. (1999) ESPript: analysis of multiple sequence alignments in PostScript. *Bioinformatics 15*, 305–308.
45. Thompson, J. D., Higgins, D. G., and Gibson, T. J. (1994) CLUSTAL W: improving the sensitivity of progressive multiple sequence alignment through sequence weighting, position-specific gap penalties and weight matrix choice. *Nucleic Acids Res. 22*, 4673–4680.